A cellulosic fibre foam as a bicycle helmet impact liner for brain injury mitigation in oblique impacts

(article starts on next page)

Research article

A cellulosic fibre foam as a bicycle helmet impact liner for brain injury mitigation in oblique impacts

Florian Feist [a],[*],[1], Markus Wagner [a], Georg Baumann [a], Stefan Spirk [b], Veronika Biegler [c], Qixiang Jiang [c], Tiina Nypelö [d],[e]

[a] Graz University of Technology, Vehicle Safety Institute, Crashworthy Biobased Composites, Inffeldgasse 13, 8010 Graz
[b] Graz University of Technology, Institute for Bioproducts and Paper Technology, Inffeldgasse 23, 8010 Graz
[c] University of Vienna, Institute of Materials Chemistry and Research, Währinger Straße 42, 1090 Vienna, Austria
[d] Chalmers University of Technology, Department of Chemistry and Chemical Engineering, Kemivägen 10, 41296 Gothenburg
[e] Aalto University, Department of Bioproducts and Biosystems, Vuorimiehentie 1, 02150 Espoo

ABSTRACT

Bulky cellulosic network structures (BRC) with densities between 60 and 130 g/l were investigated as a sustainable alternative to fossil-based foams for impact liners in bicycle helmets. The mechanical properties of BRC foams were characterized across a wide range of strain rates and incorporated into a validated finite element model of a hardshell helmet. Virtual impact tests simulating both consumer information and certification scenarios were conducted to compare BRC-lined helmets against conventional expanded polystyrene (EPS) designs. Results showed that BRC outperformed EPS in oblique impacts, reducing angular accelerations and velocity changes by approximately 33 %, particularly for z-axis rotations. The average risk of sustaining AIS2 injuries and concussions was lower for BRC (8 % and 34 % respectively) compared to EPS (13 % and 46 %). However, BRC helmets exhibited bottoming out in certain straight impacts, potentially failing certification tests. This limitation was addressed through design modifications. The study demonstrates that cellulosic fibre network structures have the potential to replace fossil-based foams in bicycle helmets while providing adequate protection and improved performance in mitigating rotational forces.

1. Background

1.1. Traumatic brain injury

A blow to the head, e.g. in a bicycle accident, can result in a traumatic brain injury (TBI). TBI is classified by severity, ranging from mild over moderate to severe. A mild TBI is also known as a concussion [1]. Moderate and severe traumas are mostly associated with bleedings (haemorrhages) inside the skull (intracranial), localized inside (intracerebral) or outside (extracerebral) the brain tissue [2]. Extracerebral haemorrhages (EH) can result from ruptures of the bridging veins (subdural haematoma, SDH), tearing of small capillaries (subarachnoid haemorrhage, SAH), or tearing of the middle meningeal artery and its branches (epidural haematoma, EDH).

---

* Corresponding author.
E-mail address: florian.feist@tugraz.at (F. Feist).
[1] Present Addresses: Vehicle Safety Institute, Graz University of Technology, 8010 Graz, Austria.

Intracerebral haemorrhages (IH) are either contusions, lacerations ("bruising of the brain") or diffuse axonal injury (DAI). The contusion is localized on the struck and/or non-struck side, called coup and contrecoup site, respectively. DAI results from shearing/stretching of the axons at the junction between grey and white matter, which differ in terms of density and mechanical properties [3].

The type of injury is linked to the type of loading: While EDH (which occurs seldom) and contusions result from linear kinematics, DAI and SDH mainly result from rotational kinematics [3] (Fig. 1). Brain matter is resistant to compression, but very susceptible to stretching and shearing [4,5]. Stretching and shearing of the brain matter are also the consequence of mechanical constraints of the brain inside the skull (bony vaults, membranes and bridging veins/arteries) and the varying physical properties of the brain matter itself (anisotropic, multiphasic) (Fig. 1) and its morphology (the raised and folded structure, denoted as gyri and sulci). The relevance of rotational loading and resulting shear strains for the occurrence of TBI and DAI specifically was readily shown in the 1940s [6], however, only relatively recently these findings have been taken into consideration in the design of head protection gear and its testing.

1.2. The relevance and characteristics of oblique impact

In animal models, it was shown that head rotations induced by tangential loading consistently result in concussion, while normal loads do not produce such effects [7,8]. In a detailed reconstruction of 26 bicyclist accidents involving head injuries, the mean impact velocity was 6.8 ± 2.7 m/s, with tangential components measuring 3.4 ± 2.1 m/s [9]. These measurements suggest an average impact angle of $33 \pm 20°$. Similarly, another study analyzing 22 reconstructed bicycle accidents reported head impact angles of approximately 40–50°, with impact velocities ranging from 6 to 7 m/s [10]. The high relevance of oblique impact was also shown for motorcycle, and equestrian accidents [11].

1.3. Epidemiology of DAI and SDH

A cohort study utilizing magnetic resonance imaging (MRI) demonstrated that DAI is diagnosed in approximately 75 % of patients with non-fatal moderate and severe head injuries, with half of these cases presenting a combination of DAI, contusions, and hematomas [12]. Post-mortem neuropathological studies have further corroborated these findings, establishing DAI as one of the most common and impactful pathologies in moderate to severe TBI [13]: In all histological samples showing limited focal changes, such as petechial hemorrhages, DAI manifests as axonal swelling or beading [13]. DAI has also gained recognition as the primary underlying pathological mechanism in mild TBI, including concussions [14,15]. This suggests that axonal injury plays a crucial role across the spectrum of TBI severity.

In the context of bicycle-related severe head injuries, SDH demonstrates a high prevalence. Approximately 50 % of all such injuries involve SDH, with this rate increasing to about 75 % in individuals aged 65 and older [16], highlighting the particular vulnerability of older adults to this type of injury in bicycle-related accidents.

1.4. Helmet effectiveness

The benefit of wearing bicycle helmets and legal obligations to wear a helmet have been intensively and controversially discussed over the last decades in literature and policy making entities [17,18]. The most recent data, based on case-reconstructions [19,20], experiments [21] and case-control-studies, however, draw a clear picture: non-helmeted bikers have higher rates of mortality
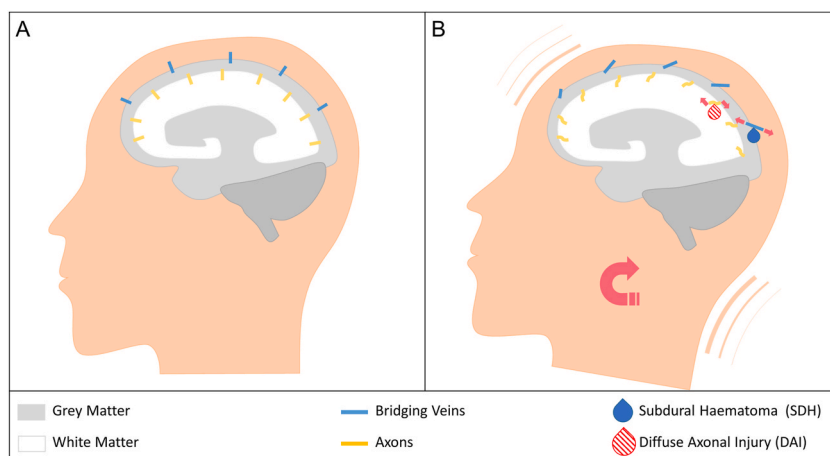
Fig. 1. DAI and SDH: Injuries resulting from rotational kinematics. (A) Prior to impact and (B) during impact: stretching of veins, shearing and stretching of axons, resulting in subdural haematoma and intracerebral haemorrhages.

(odds-ratio, OR = 2.4) and a higher risk for severe head injury (OR = 2.3) [22]. Even higher benefits are reported in a meta-analysis covering multiple dozen studies [17,18] where an OR of 3.2 and 2.9 for fatal and severe head-injury respectively are reported [17]. However, helmet usage does not reduce the rate of mild TBI [23] and seemingly increases the rates of cervical spine injury [22].

1.5. Helmet safety performance certification and assessment

Bicycle helmets sold in Europe must comply with the European standard EN1078. Similar certification standards exist for other national and transnational markets, e.g. CPSC in the USA: The helmet is placed onto a rigid headform, which is equipped with translational accelerometers. The headform and helmet are dropped from heights between one and 2 m onto a rigid anvil, which is either flat, rounded (spherical) or curbstone-shaped. To pass the test the peak acceleration must not exceed a performance criteria (between 200 and 300g), depending on drop height, anvil-style and standard. None of the current bicycle helmet certification tests take into consideration rational head motion [24] nor the effect of upper body and neck [25], though there is ongoing work within European standards organization (CEN/TC158).

As of now, only consumer information tests evaluate the performance of helmets in oblique impacts and the associated rotational kinematics – such as Certimoov (Cmv) [26], the Virginia Tech helmet rating (VThr) [27], Folksam Cykelhjälmar test (FCt) [28] and Länsförsäkringa (LF) [29]. In Cmv and FCt the protection level is (partly) evaluated through a finite-element based „Brain Biomechanical Model" – while the VThr relies on the kinematic-based R criteria, combined through the STAR rating. These rating procedures sometimes return contradictory results, where one helmet is rated very good in one test – and average in another [30]. Please refer to the Supplementary Material for a conceptual view of helmet safety performance certification and assessment.

1.6. Head injury risk assessment

The safety afforded by a helmet (or more precisely the accelerations measured in the headform) can be assessed in two ways. By applying kinematic-based metrics (as is done in the VThr and EN1078) or by prescribing the measured accelerations to a biomechanical finite element model of the head and brain (as is done in Cmv and FCt) and then evaluating element-based strains and pressures (see Supplementary Material).

Over the last six decades, a huge number of kinematic-based metrics (or criteria) have been developed: Probably the most known is the Head Injury Criterion, HIC [31] assessing the translational motion only and taking into account the regressive correlation between the tolerable acceleration and the exposure duration. The HIC was very often (mis)used for assessing traumatic brain injury [11], but was found ineligible for assessing other injury than skull fracture [32] – for which it was developed initially [33].

In the mid-1980s the Generalised Acceleration Model for Brain Injury Threshold, GAMBIT [34] was assessing the combined angular and translational acceleration. In the 2000s the Power Index, PI [35] was the first to consider the directionality of the motion, taking into account the higher sensitivity to one loading direction over the other. From the 2010s a number of criteria have developed based on numerical studies employing biomechanical models of the brain – like the Brain Injury Criterion, BrIC [36]. In numerical head brain models, strain-based criteria, like the cumulative strain damage measure (CSDM) and maximum principal strain (MPS), have became so well established that the most recent kinematic criteria (like Diffuse Axonal Multi-Axes General Evaluation, DAMAGE) estimate these measures, i.e., they are metamodels of the detailed finite element models [37]. In that way, the detailed brain model in consumer tests might get replaced by these meta functions. A comprehensive list of the criteria [27,31,34–49], their acronym and formulas can be found in the Supplementary Materials.

These metrics are functions of the accelerations or velocities. Simpler are peak values such as: peak resultant linear acceleration (PLA), peak angular acceleration (PAA), and peak angular velocity (PAV). A very recent study employing eight numerical models of the brain revealed a low (<0.8) correlation coefficient (R^2) for PLA, HIC, STAR (and R) and a high correlation for PAA, BrIC, UBrIC, DAMAGE with brain strains. PAA was found to have an R^2 above 0.8 in only two brain models and is believed to correlate with injury outcome in longer duration pulses, e.g. automotive collisions, but not in short duration helmet impacts (10–20 ms) [32].

1.7. Helmet design

A bicycle helmet consists of the outer shell, the impact liner, an optional slip liner and a comfort liner. The outer shell prevents penetration, provides structure to the inner liner preventing disintegration upon hard contact [50] and is spreading load in localized loading [51]. The outer shell is mostly made from plastics, namely polyvinyl chloride (PVC), acrylonitrile butadiene styrene (ABS), polyethene terephthalate (PET) and polycarbonate (PC) [52]. There are two outer shell designs: A thick, stand-alone hardshell (mostly made from ABS), to which the impact liner is glued (also then often denoted as "skater helmet") – or a thin, flexible in-mould shell (mostly made from PC), to which the impact liner is adhered in the process of foaming the impact liner [49].

The impact liner is comparatively soft and compliant, increasing the distance and time to stopping the head and thus reducing the peak loads and accelerations. It is commonly made from synthetic foams, with expanded polystyrene (EPS) being the most common, but sometimes expanded polypropylene (EPP), ethyl vinyl acetate (EVA) [53] or flexible polyurethanes (PUR) are employed. These liners may feature gradient densities [54], as they can provide improved energy absorption [55].

A slip liner can be present between the impact liner and the comfort liner and reduces the rotational peak accelerations as well as the rotational velocity change. Last but not least, the comfort liner, is made from soft elastic or viscoelastic foams, improving the fit (to the non-flexible impact liner) and the feel (of the circumferential fitting straps).

While this design seems simple and straightforward, there has been a lot of innovation in the last two decades, mainly related to the

(1) reduction of angular momentum and associated injury like DAI. Other research and development has focused on (2) higher energy absorption/more crush space, (3) multi-impact protection, (4) adaptability to impact severity, (5) stowability, and (6) product sustainability.

1.8. Reduction of angular momentum

Reducing the tangential shear traction upon impact - either between (a) the hardshell and the road-surface, (b) within the impact liner or (c) between the head and the impact liner - can help to reduce the angular momentum acting on the head. Please refer to the Supplementary Materials for a more in-depth description of the individual systems.

A meta-study on helmet impact tests with and without advanced injury mitigation systems, such as MIPS, SPIN, ODS, WaveCel, and AIM, showed that these "[…] performed significantly better than the conventional helmets for kinematics-based metrics at low impact velocities and low impact angular momentum." [56].

Fig. 2 shows a systematic overview on the innovations aimed at reducing the angular momentum due to oblique helmet impacts by underlying mechanism and concept.

1.9. Sustainability in helmet design

Decreasing the environmental footprint of products during their life cycle has become a hot topic – also in helmets [52]: The *Kranium* helmet [57], inspired by the bone structure of the woodpecker, uses interlocked corrugated paper strips. The *Paper Pulp* helmet is made from discarded newspapers [58,59] and is waterproofed through food safe additives. It was designed for single use in bike-sharing. The *EcoHelmet* also relies on waterproofed recycled paper in a radial honeycomb pattern but is foldable along its longitudinal axis like a book [60]. That corrugated paper and honeycomb helmets would perform well in terms of safety performance, which has been shown in numerical simulations [61]. The *Cellutech* helmet [62] was developed based on materials from the forest: The impact liner relies on the nanocellulosic foam *Cellufoam™* (now *Papira®*).

Cork is a natural grown cellular structure and therefore is considered a suitable impact energy absorber in helmets [50–52,63]. However, the density of lower weight (micro-agglomerated) cork is two to four times that of common EPS liners used in helmets [51]. To cut the weight to below 2 kg, cork is used in combination with EPS (with 20–40 % of cork) [50]. Cork is thought to handle multi-impacts well [50,63] – but thus requires small grain sizes [64]. Its multi-impact performance can be further improved through
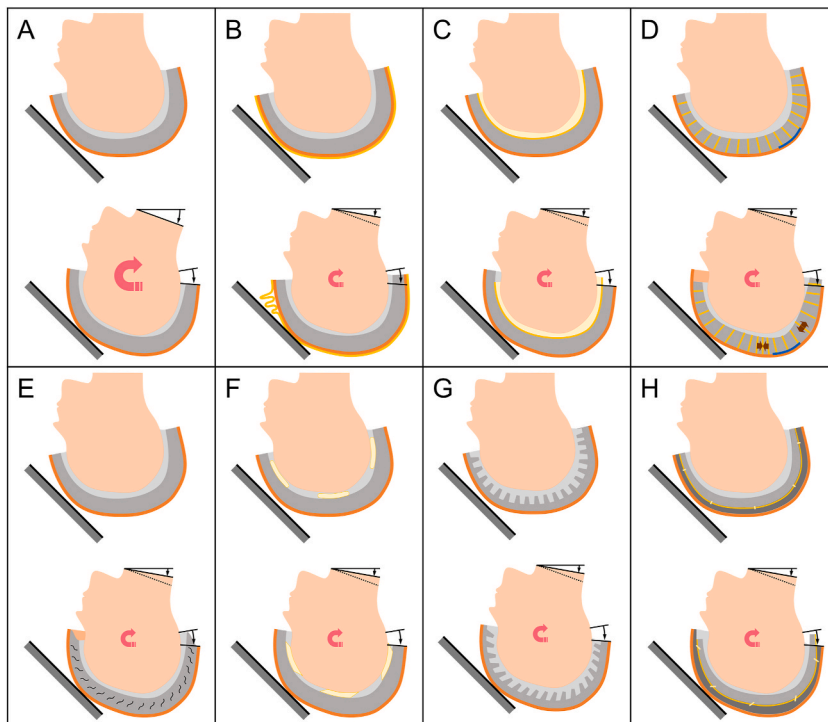

Fig. 2. Schematic overview on the innovations w.r.t. the reduction of angular momentum in helmets due to oblique impact: (A) conventional helmet, (B) tearable outer skin (e.g. *Lazer SuperSkin*), (C) inner slip layer (e.g. *MIPS*), (D) anisotropic impact liner with low tangential stiffness/strength (e.g. *AIM*), (E) impact liner with low shear stiffness/strength (e.g. *WaveCell*), (F) viscous and/or fluid filled comfort liner (*SPIN*), (G) shear-stiffness/strength reduced impact liner through lamellation of isotropic material, (H) two layered impact liner, connected through a suspension system (e.g. *ODS* and *Brainguard*).

shear-thickening fluids [65]. Cork's energy absorption capability does not degrade at moderately elevated temperatures (50 °C) [66, 67] – and it shows a high viscosity, highly hysteretic and load-rate dependent behaviour [68].

MyHelmet is a helmet with a mycelium-based impact liner. Mycelium is a network structure formed by fungi to transfer nutrients, similar to the roots of a plant [69]. Mycelium is versatile in mimicking other materials, by changing strain/species, growth substrate and manufacturing process [70]. In *MyHelmet* the mycelium is grown in a hemp-flake substrate, thus reinforcing the mycelium network, as the fibres weave together [69].

Cellulose is an inexhaustible natural polymer, which can be abundantly found in the cell walls of trees and plants [93]. Cellulose foams are a relatively "young" material [91] and there is a plethora of research dealing with its potential application as thermal insulation [92], sound absorber [94], fluid adsorber, scaffold for phase change materials, hydroponic, filtering, electromagnetic shield and electrical energy storage. Furthermore, cellulose foams are considered a substitute for non-biodegradable synthetic foams like EPS for cushioning purposes in the packaging industry [95,96].

This study investigates the suitability of cellulose foams as an impact liner in a helmet – based on legislative and consumer information testing.

2. Methods

Cellulosic foam samples were characterised in compression at various strain rates (ranging from roughly 0.004 s^{-1} to 700 s^{-1}) and in tension quasi-statically. With the stress-strain-strain rate tables a material model was established in LS-Dyna. The material model was validated against drop tests with a rigid spherical impactor. Once validated, the material model was employed in a validated and publicly available helmet model. The numerical model was used to conduct a study to identify, whether the helmet would pass the certification test according to EN1078 – and how the helmet would perform in a test inspired by a consumer protection test – in comparison to the baseline helmet with an EPS impact liner.

2.1. Material preparation

The foams for mechanical characterization and impact testing were made by frothing bleached softwood kraft pulp dispersed in an aqueous solution containing (sodium-)carboxymethylcellulose (CMC) (5 wt% in water) and sodium dodecyl sulphate (SDS) (0.5 wt% with respect to the dry fibre weight) as a viscosity modifier and foaming agent/surfactant, respectively. Frothing was performed until a desired density was reached. All components were frothed using a kitchen mixer on full speed (1000 W, Kenwood) until a desired air volume of 30, 20 or 12 % for densities of 60, 100 and 130 kg/m^3 was introduced. The wet foam placed in a mould ($10 \times 10 \times 2$ cm^3 for generating drop test and compression samples and $31 \times 31 \times 2$ cm^3 for generating tension samples), was dried in a laboratory oven at 80 °C until the moisture content was less than 10 %. The specimens were conditioned prior and after further processing at room temperature (RT) and 65 % relative humidity (RH). The foams were cut to the desired shape using an electric fret saw. For a more comprehensive description of material preparation and characterization, refer to Wagner et al. [69].

2.2. Material characterisation: quasi-static compression

Quasi-static compression characterisation was conducted on a universal testing machine Z020 by ZwickRoell equipped with a "xforce K" loadcell with 20 kN nominal force capacity. Compression tests were conducted according to ISO 844 for rigid cellular plastic. The specimens were cut to $50 \times 50 \times 20$ mm^3 (Fig. 3, left), preloaded to 2 N and tested at a rate of 5 mm/min – until a force of 15 kN had been reached.

2.3. Material characterisation: quasi-static tension

Tensile tests were conducted according to ISO-1926 for cellular plastics. The specimens were dog-bone shaped, with an overall
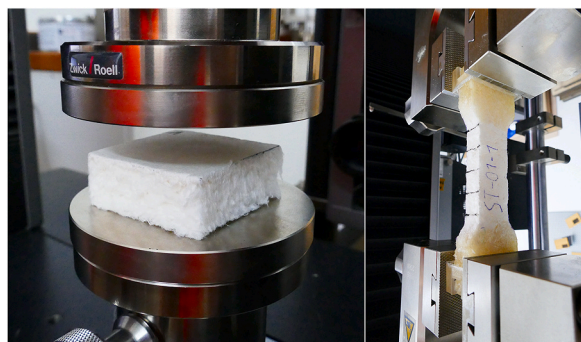

Fig. 3. Quasi-static compression test (left) and tension test (right).

length of 150 mm and width of 40 mm. The nominal length and width were 55 by 25 mm^2. The clamp section of the specimen was reinforced through epoxy resins (Fig. 3, right). The specimens were preloaded to 2 N and tested at 20 mm/min – until a 95 % decline in force was detected.

2.4. Material characterisation: dynamic compression

High strain rate characterization tests were conducted on a self-developed Split-Hopkinson bar for low impedance materials. For a detailed description of the test device refer to Baumann et al. [97]. The specimens were cut to a cylindrical shape with a diameter of 20 mm and a thickness of 20 mm (Fig. 4). In terms of environmental conditions, the samples were climatised at 23 °C and 70 % RH (relative humidity) for at least 12 h prior to testing. The foams were prestressed between the incident and transmission bar to approximately 2 N. The striker bar was pre-tensioned to 50 and 80 kN, resulting in a strain rate of approx. 400 and 700 s^{-1}, and a maximum engineering strain of 30 and 50 %. The strain-rates of 400 s^{-1} and 700 s^{-1} correspond to test speeds of 9.1 m/s and 14.5 m/s respectively. Slight deviations in effective strain rate and maximum compression result from the different material strength and energy uptake. For a detailed description of the characterization at high strain rate refer to Wagner et al. [69].

2.5. Impact test with spherical impactor

A 3.5 kg child headform impactor according to the European Automobile Manufacturers Association ACEA safety test procedure was equipped with triaxial accelerometers (Endevco 7264C) with a measurement range of 5000 m/s^2. The compliant skin was removed. The impactor was dropped onto the foam specimens at 3.13 m/s (Fig. 5). Each test was repeated five times for each foam density group (60, 100 and 130 kg/m^3). The impactor was unguided during the free fall phase. The specimens were placed on a massive flat solid steel plate. The resultant acceleration signal was filtered with a low-pass Butterworth filter (CFC 1000). The PLA, HIC and the coefficient of restitution (COR) were calculated. The latter was used to calibrate the 'hysteretic unloading' in the material card. All specimens were 20 mm thick and 100 × 100 mm^2 wide – i.e. have been used as moulded with a skin along their perimeters. The foam's growth axis and thickness were oriented parallel to the impact direction. As the foams were manually made, thickness and density showed a variation of ± 10 %. Thickness variations were accounted in the validation of the numerical model. For reference, tests have also been conducted on synthetic foams (EPS, EPP, PVC, PET) with an identical sample size but almost no dimensional variation.

2.6. Material modelling

Both, the baseline EPS impact liner and the cellulosic impact liner were modelled employing Mat83 in LS-Dyna, which obeys to the unified constitutive laws by Chang [70] considering the effect of compression strain rate, tension strain, and shear strain for low-density, highly hysteretic foam materials with very low Poisson's ratio.

A double-logarithmic interpolation between the stress-strain-rate tables was selected to minimize interpolation errors upon internal rediscretization [71], which can occur if the range of strain rates (and yield stresses) spans several orders of magnitude as in the given case. Three separate material cards have been created for 60, 100 and 130 g/l of the cellulosic foam. Following default settings have been selected for all material cards: An optional contact bulk modulus ('KCON' = 0.1 GPa), greatly exceeding the initial bulk modulus was selected to allow for a conservative time-step and robust calculation. The minimum strain rate was selected equal to the quasi-static strain rate ('MINR' = 4e-3 s^{-1}), below which no extrapolation of strain rate effects occurs. Damping has been selected relatively large ('DAMP' = 0.4). Strain rate effects were considered in unloading, too ('RIULD' = 1). Strain rate behavior has been defined over three individual curves, covering the strain-rates 4e-3, 400 and 700 s^{-1}. Extrapolation for higher strain rates was not restricted ('MAXR' = 0). For tension a cut-of-stress was defined, i.e. tensile stresses are not dropping to zero once tensile strength is reached, but they are not further increasing either. Individual card settings are summarized in Table 1. Other parameters were left to default. The yield curves obtained in dynamic material testing and input to the material card are shown in the results section.
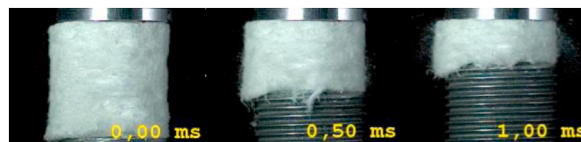

Fig. 4. Exemplary high-speed sequences of a dynamic compression test at a strain-rate of 700 s^{-1} (0 ms, 0.5 ms and 1.0 ms).

Fig. 5. Drop test (-6 ms, 4 ms and 40 ms). Observe the permanent deformation in unloading.

Table 1
Parameters in material model.

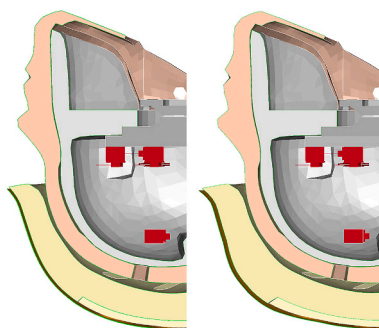| Density	Young's modulus	Tension cut-off	Hysteretic unload	Shape
[g/l]	[kPa]	[kPa]	[ ]	[ ]
60	74	102	0.01	5
100	194	323	0.01	6
130	780	399	0.01	6

Fig. 6. Morphing of helmet in the forehead region: baseline (left) and morphed (right).

2.7. Helmet modelling

The helmet used in this study has been validated previously [25] – and is publicly available through GitHub [72]. The helmet is a so-called hardshell helmet. The outer hardshell from ABS is assumed elastic-plastic (with a Young's Modulus of 3 GPa and yield strength of 42 MPa). A linear damage model with an initiation strain of 6 % and a failure strain of 42 % is assumed. Strain-rate effects are considered. All contact interactions are using a soft-constrained contact. The static and dynamic coefficients of friction were assumed identical: 0.35 between head and helmet, 0.5 between helmet and anvil, and 0.3 between hardshell and foam. Other than in the initial study [83], the inertia beam, resembling the effects of neck and upper body, was removed. It must be noted, that the impact liner is only adhered locally (at the area of the crown) to the hardshell – allowing for sliding between liner and shell elsewhere.

A morphological variation of the baseline helmet was included in this study, to accommodate a thicker foam layer in the forehead region. The morphing process was carried out using LS-PrePost software. The outer hardshell and the two outermost foam layers were constrained to a spherical morphing geometry having 24 control points placed around its perimeter. The control points in the front section were shifted 10 mm in the longitudinal direction, resulting in a maximum thickness increase of the foam of 8 mm (see Fig. 6).

The EPS foam density of the baseline helmet amounts to 70 kg/m³. Further investigations were conducted on EPS liners with lower densities, specifically 35 and 50 kg/m³. The stress-strain relationships observed across these three densities adhered to the principles elucidated by Cui et al. [88], based on earlier work by Schraad and Harlow [89] concerning a constitutive law for disordered cellular materials.

2.8. Design of experiments

The helmet was tested in eleven impact constellations, of which seven are replicating the consumer information tests (Cmv, FCt and LF) and four the certification test according to EN1078:2014–04 [90] (see Fig. 7). In EN1078 the test engineer can select critical impact constellations. Here, the impact points were selected based on the results of the consumer information tests (01 through 07): The impact to the crown was found to return the highest PLA in the EPS baseline helmet and the impact to the front returned the highest PLA in the BRC helmets. Accordingly, these impact points were selected and tested against the flat (08, 10) and the curb stone-shaped anvil (09, 11).
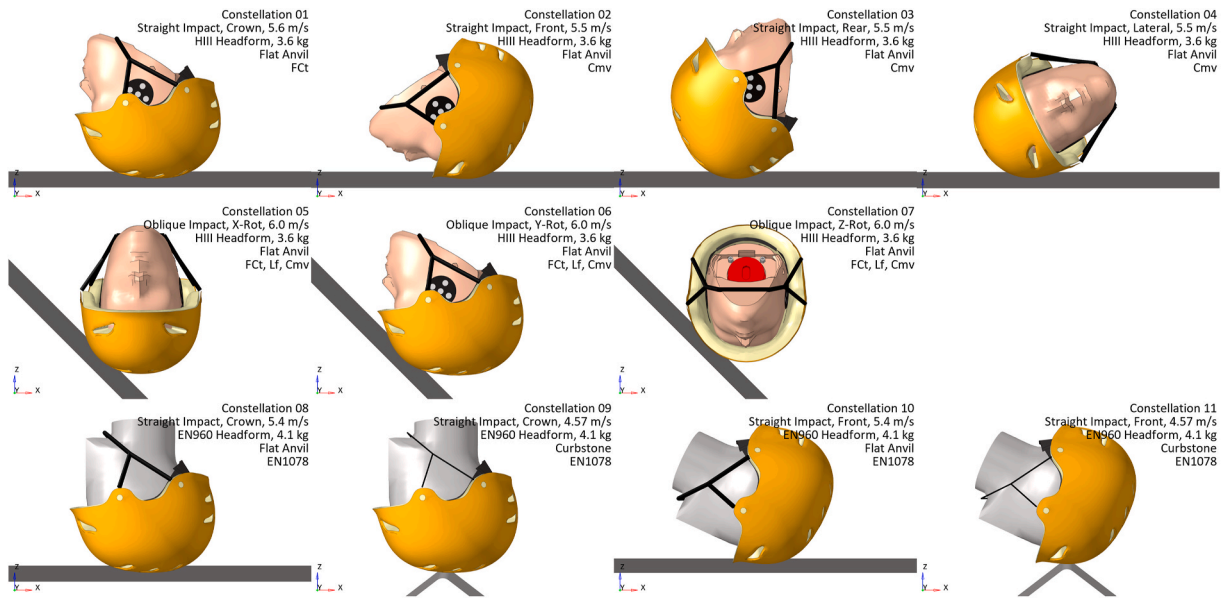
Fig. 7. Head Impact Constellations: impact point, impact velocity, headform type and mass. First two rows: consumer information tests. Last row: certification test. First and last row: straight impacts. Middle row: oblique impacts.

The kinematic data was postprocessed, and the following metrics were analysed: The peak angular acceleration (PAA), the peak angular velocity (PAV), the peak linear acceleration (PLA), the Head Injury Criterion (HIC), the Brain Injury Criteria (BrIC). Further metrics estimating the strains in the brain, the Maximum Principal Strain (MPS) and the CSDM (Cumulative Strain Damage Measure), were evaluated: Universal Brain Injury Criterion (UBrIC), Diffuse Axonal Multi-Axes General Evaluation (DAMAGE), and the BrIC-refit. Further the risk for concussion (R) was calculated. For the formulas refer to the supplementary material.

3. Results

3.1. Dynamic material characterization

The strain rate amplification (averaged over the first 30 % of compressive strain) was found to increase linearly with the (linearly plotted) strain rate. The strain rate amplification decreases with density. Highest amplification is observed with the lower density samples (Fig. 8, left). The strain rate amplification was found to be not constant over strain: It appears that the amplification is highest at the onset of compression, and levels off at strains beyond 30 % (Fig. 8, right).

The high strain rate data of the material is only available up to a volumetric strain of approx. 30 and 50 %, respectively. To obtain the stress-strain behaviour beyond these strains for the material card yield curves (Fig. 9) a constant amplification was assumed. This is indicated by the dashed lines.
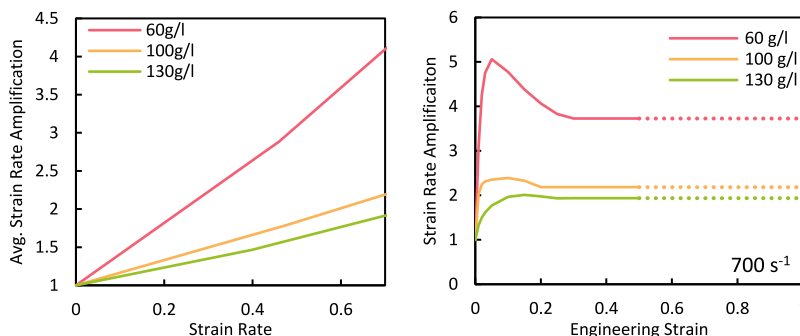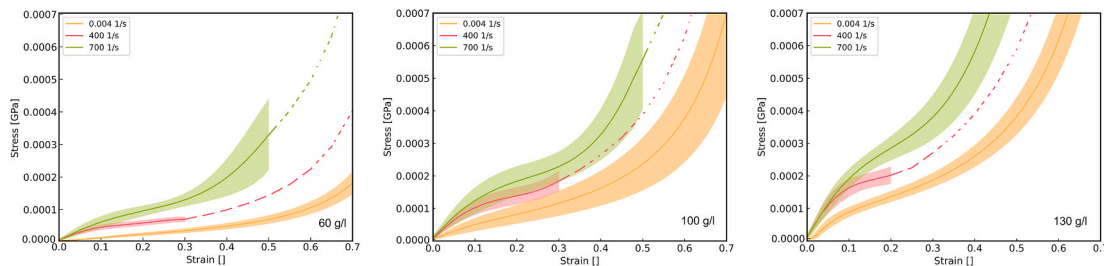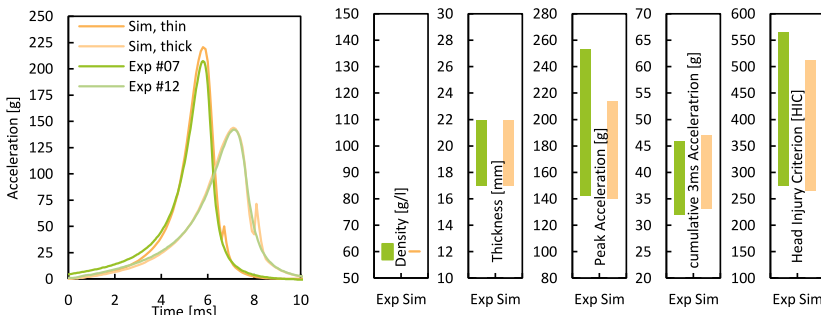

Fig. 8. Strain rate amplification as function of strain rate (left), and as a function of strain (right). Dotted lines indicate the assumed extrapolation.
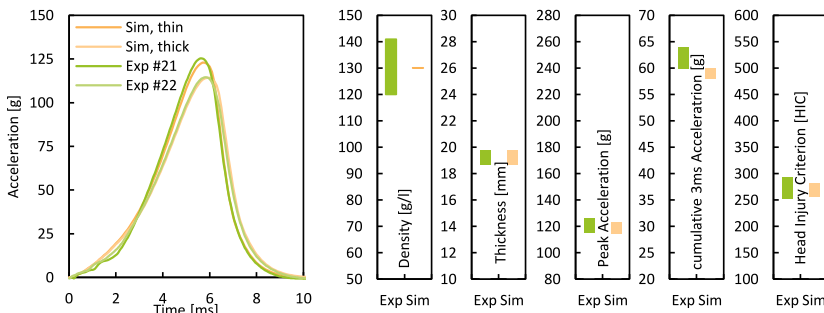
Fig. 9. Stress-strain-strain rate curves for three foam densities. Dashed lines indicate the assumed extrapolation and shaded areas indicate the standard deviation of the stress-strain curves.

Fig. 10. Validation of BRC foam with a density of 60 g/l.
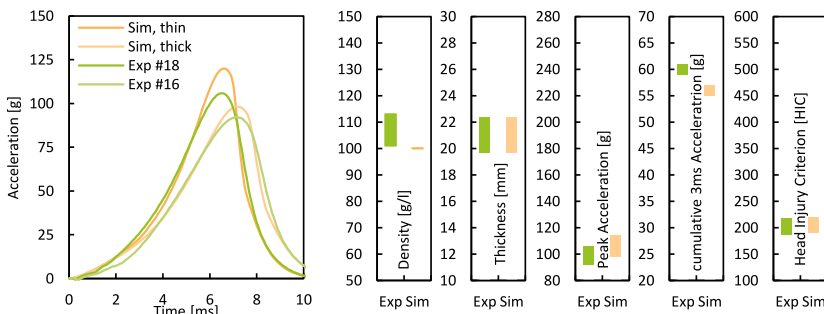
Fig. 11. Validation of BRC foam with a density of 100 g/l.

Fig. 12. Validation of BRC foam with a density of 130 g/l.

3.2. Validation of material model

The line diagrams show the acceleration-time signals of the simulation (orange) and experiment (green). The dark and light-coloured lines show the results in drop tests against the thickest and thinnest sample of each density group (Fig. 10–12). The bar diagrams show the spread of density, thickness, peak linear acceleration, cumulative 3 ms value and head injury criterion. The lowest density specimen showed the highest variation in terms of thickness (Fig. 10), but also in terms of peak accelerations, HIC criteria and 3 ms value, as bottoming out occurred in some tests.

3.3. Comparison against synthetic foams

The maximum acceleration values of the three density groups of the BRC foam are compared with the values obtained from the synthetic foams, including EPS, EPP, PVC and PET, see Fig. 13. It is evident that the scatter of the cellulose foams, particularly the 60 g/l cluster, is considerably higher than the scatter of the synthetic foams, which exhibit a negligible degree of dispersion. The high degree of scatter observed in the cellulose foam samples can be partially attributed to their considerable variation in thickness, but also to their less homogeneous fiber network structure. A comparison of the maximum acceleration values on a mean value level revealed that the EPS and EPP foams exhibit lower values than the cellulose foams, whereas the PVC and PET foam samples demonstrate higher values. The confidence intervals for the cellulose foams are as follows: 60 g/l (134.9, 188.5), 100 g/l (89.2, 109.6) and 130 g/l (113.5, 129.5) - see Fig. 13.

3.4. Virtual consumer information test

Fig. 14 summarizes PLA, PAV and PAA of the EPS baseline helmet (reddish colours) – and the helmets with BRC impact liner (bluish colours). Except for impact constellation 2, where bottoming-out of the BRC foam occurs, the BRC impact liners consistently returns similar or lower peak linear and angular accelerations. In straight impact constellations (1 through 4), peak angular velocity is higher with the BRC impact liner. In the oblique impact constellations (5 through 7), however, the BRC liner shows lower PAV as compared to the EPS liner – in particular in impact constellation 7 (rotation about z-axis). Apparently, there is a difference, whether the angular motion is induced by a radial force (1 through 4) – or by a tangential force (5 through 7), where the low shear stiffness and the lower tangential stiffness of the BRC foam seems beneficial.

Decreasing the density of the EPS (compare dark vs lighter colours), leads to a decrease in peak linear acceleration. The same holds true for the angular acceleration, with the exception of impact constellation 2. On average over all constellations, the BRC 100 g/l returns lower peak linear accelerations (158 vs 179 g) and angular accelerations (5 vs 8 krad/s^2) than the EPS 70 g/l baseline. The average values for EPS 35 g/l are 137 g and 6 krad/s^2, i.e. lower than the baseline helmet. The average values for the morphed BRC 100 g/l helmet are 141 g and 5 krad/s^2. The average PAA across all constellations amounts for 23 rad/s^2 for all 7 helmet variations.

Remark: The PLA threshold of 250 g, based on EN1078, is shown through a dotted red line.

The maximum principal strain (MPS) in the brain matter can be estimated with the help of BrIC-refit, uBrIC, Ci, and Damage (Fig. 15). BrIC-refit is based on angular velocity, DAMAGE is based on angular accelerations, while uBrIC and Ci considers both, angular acceleration and velocity. The red dotted line shows the threshold value corresponding to a 50 % risk for a moderate injury (AIS2) [73]. Except for Ci, all criteria return fairly similar absolute values: They consistently show, that constellations 4 through 7 return the highest MPS values. As readily indicated, the BRC liner performs better in the oblique impacts – but worse in the straight impacts - than the EPS baseline. The BRC liner performs extraordinarily well in constellation 7. The helmet shows more structural deformation, but also the foam reduces form locking effects (compare deformations of the helmet and rotational displacement of head in Fig. 17). That Ci returns considerably different results as compared to uBrIC and BrIC-refit is surprising, given that the critical values were determined by one author [37] using the same FE model (SIMon).

While the influence of EPS impact liner density was very consistent for PLA across all impact constellations (Fig. 15), the same is not visible on the estimated brain strains. The effect of foam density on the brain strain estimated by BrIC-refit, DAMAGE and uBrIC seems
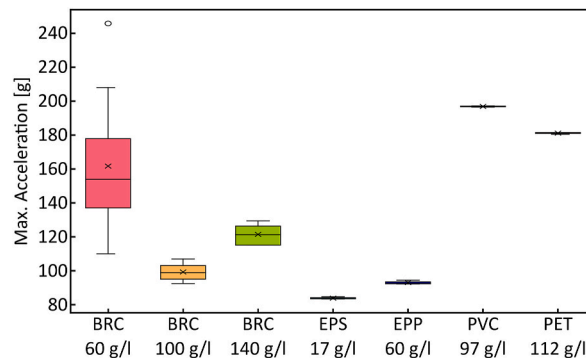

Fig. 13. Comparison of the maximum acceleration of the cellulose foams with other state of the art foams including EPS, EPP, PVC and PET.
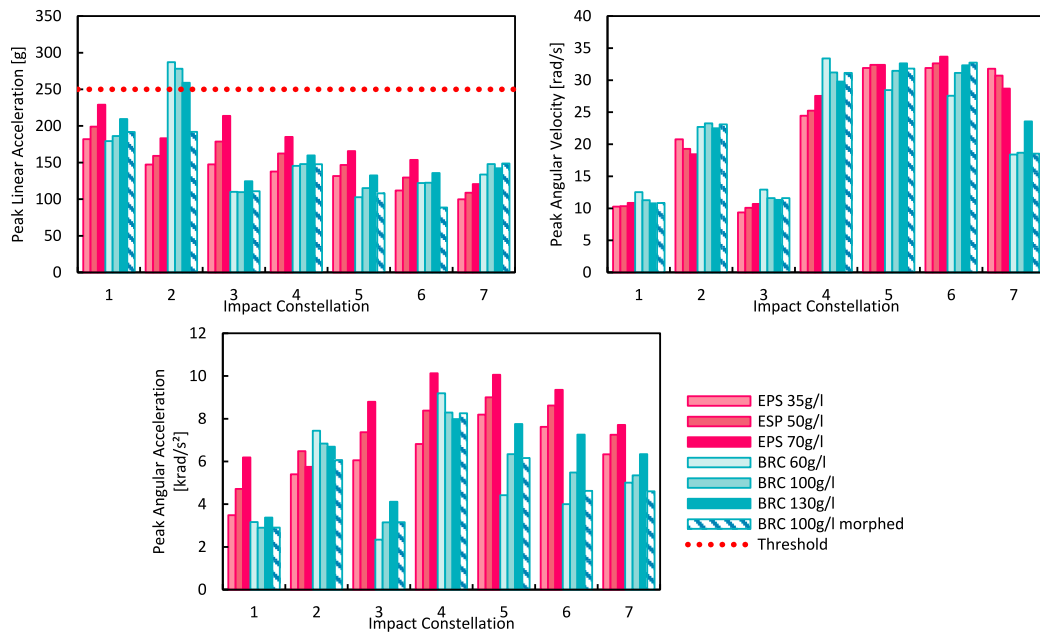
Fig. 14. Peak Linear Acceleration, Peak Angular Velocity and Peak Angular Acceleration – in virtual consumer tests.
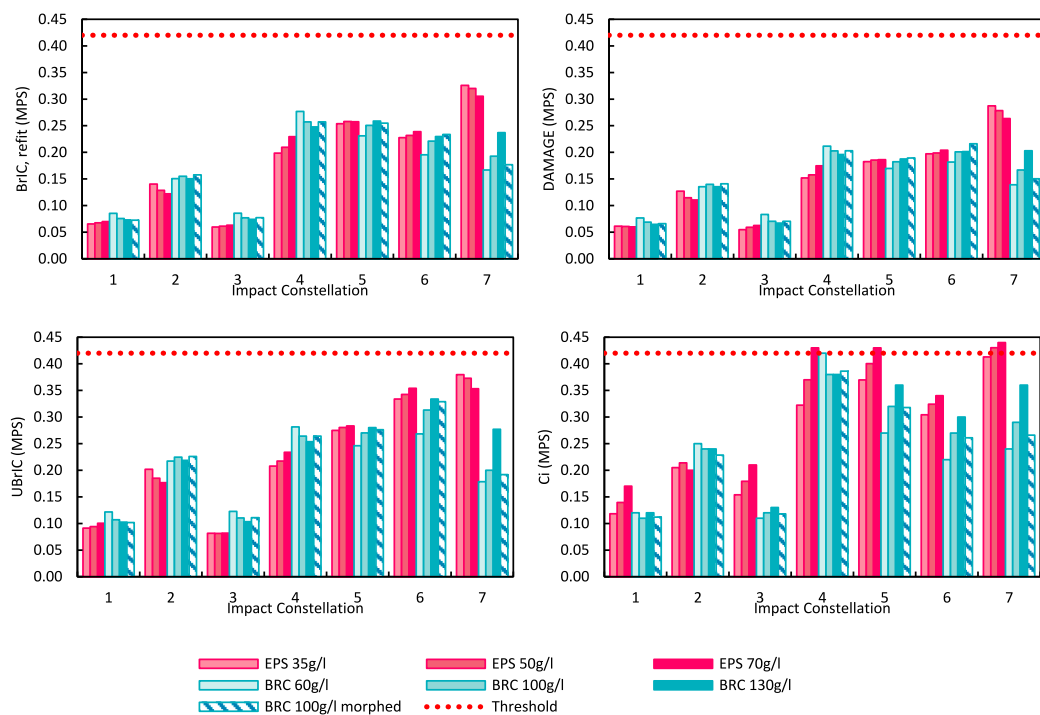

Fig. 15. Estimation of the Maximum Principal Strain (MPS) in the brain matter – in virtual consumer tests.

very limited. The only remarkable difference is visible in impact constellation 7, between BRC and EPS helmets.

The risk for injury can be calculated from the MPS (in the given case from those calculated with DAMAGE), using the AIS 1 and 2 risk functions established by Takhounts et al. [36]. Another approach is based on R, the underlying criteria of VTHr. Observe that R is a function of linear acceleration and rotational velocity – while DAMAGE is considering angular kinematics only. Also, R is based on real-world football accidents, while DAMAGE is based on FE simulation.

R shows a substantial risk for concussion in constellation 2, due to the bottoming out of the BRC helmet (Fig. 16 and 17, left). On the
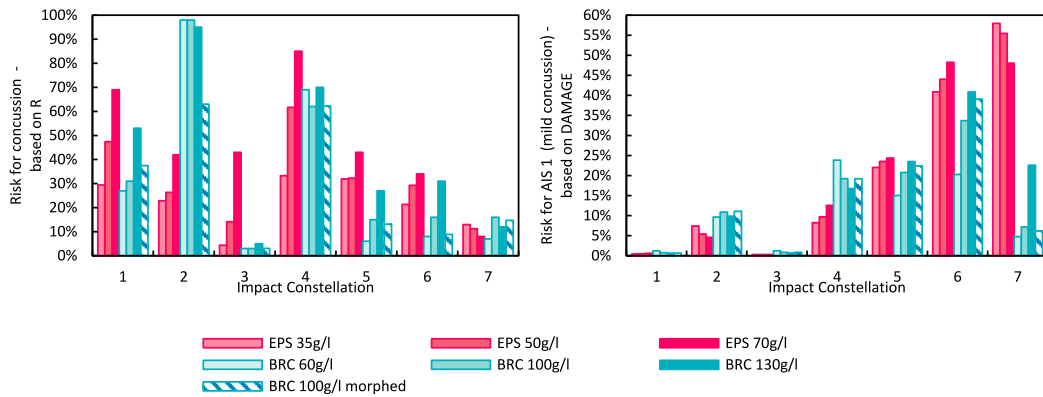
Fig. 16. The risk for concussion, based on R, and risk for AIS 1 brain injury (mild concussion), based on DAMAGE, in virtual consumer tests.
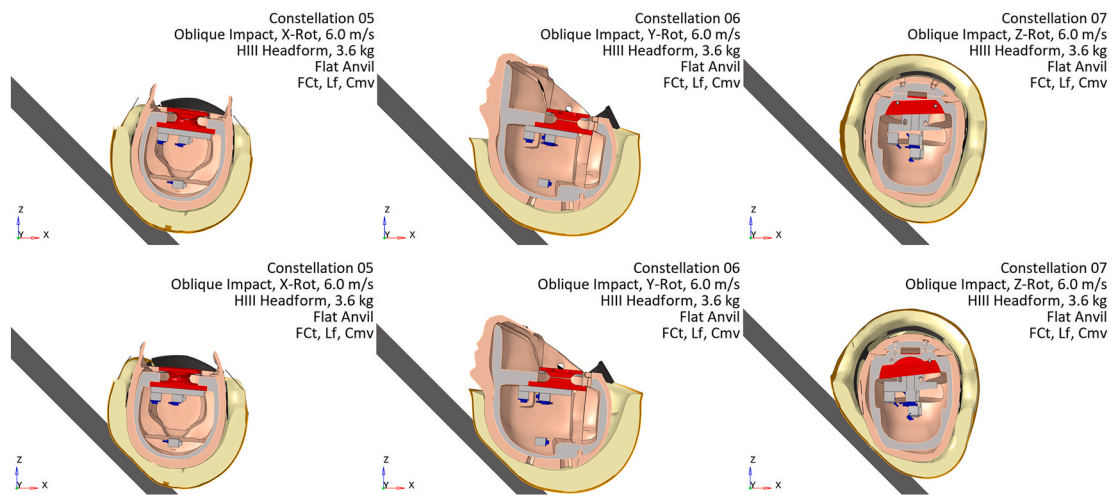

Fig. 17. Cross-sectional views of helmet deformation 10 ms after T0 in impact constellation 5, 6 and 7. Top row: EPS 70 g/l; Bottom row: BRC 100 g/l.

other hand, the injury risk (AIS1) is substantially reduced in constellation 7 with BRC (Fig. 16, right). By increasing the thickness of the helmet at the front ('morphed'), the risk for concussion in constellation 2 can be significantly decreased.

On average, the lowest risk for concussion is provided by the EPS 35 g/l (22 %), followed by BRC 100 g/l morphed (29 %), and BRC 100 g/l (34 %). The average risk for concussion with the baseline helmet (EPS 70 g/l) amounts for 46 %. The lowest average risk for minor (AIS 1 = mild concussion) and moderate (AIS2, not shown in diagram) is provided with the BRC 100 g/l (13 %) – as compared to the EPS liners with 35–70 g/l with 20 %.

3.5. Virtual certification test according to EN1078:2014–04

The EPS baseline helmet passed all four tests: In none of the constellations the PLA exceeded 250 g. This surprisingly also holds true for the lower densities of EPS. The most lightweight BRC foam bottomed-out in constellation 9, 10 and 11 (Fig. 19), causing PLA to exceed the limit (Fig. 18). When increasing the density of the BRC foam, bottoming-out is occurring in constellation 10 only. It appears counterintuitive that constellation 11 is returning a lower PLA than 10, considering the more localized loading (Fig. 19), worsening the bottoming-out. However, more energy is converted into rotational loading, i.e. higher rotational velocity change, in constellation 10.

The BRC with densities exceeding 100 g/l would pass 3 out of 4 certification tests. There are several potential approaches to overcome the BRC failing in constellation 10. One was investigated in this study, by locally increasing the foam thickness at the front-end, where the baseline helmet's impact liner is relatively thin. When increasing the foam thickness by 8 mm ('BRC 100 g/l morphed') the peak acceleration remains below 250g, i.e. is decreased by a third. This helmet passes all certification tests. Other approaches would be feasible, such as to increase the density of the foam further. However, with increasing foam density load-rate effects are reduced (Fig. 8). Alternatively, higher density cellulosic [87] layers can be introduced, that increases the initial stiffness and crush strength. As shown conceptually outlined in the Supplementary Materials, a high initial stiffness and strength is beneficial to limit the
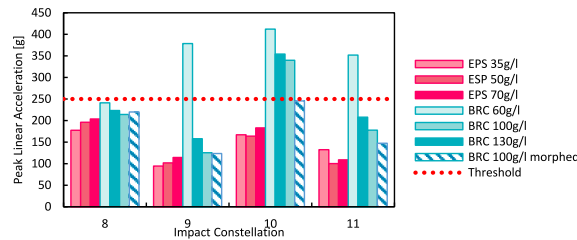
Fig. 18. Peak Linear Acceleration – in Virtual Certification Test in accordance to EN1078.
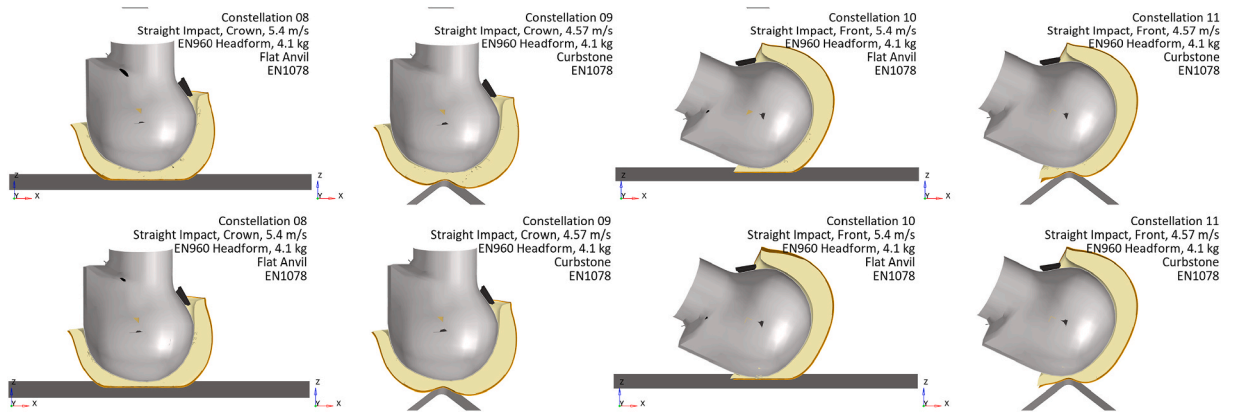

Fig. 19. Cross-sectional view on helmet deformation 4 ms after T0 in impact constellation 8, 9, 10, and 11. Top row: EPS 70 g/l; Bottom row: BRC 100 g/l.

crush depth, i.e. to reduce the required foam thickness to dissipate the initial kinetic energy. And, last, enhance the density homogeneity in thickness direction: Scans with the computed tomography showed, that the BRC foam is less dense in the middle layer [85] – which is also reported by other research groups [84]. Theoretical and numerical considerations show, that the average crush strength of the BRC foam can be improved approx. by a third when density would be homogenous over the thickness [69,86].

4. Discussion

4.1. Densification strain

Densification strain is a function of the relative density, which is the ratio of the foam density to the density of the solid it is made from, multiplied by the 'lock-up density' [74]. The latter often is assumed to be 0.6. The higher the relative density or the lower the solid density, the lower the densification strain. The solid density of cellulose is 1500 kg/m³, as compared to that of polystyrene, which is 1000 kg/m³. So, densification strains in cellulose-based network structures are 30 % higher (50 % solid density surplus, multiplied by the lock up density of 0.6) as compared to polystyrene foams. This surplus in densification strain can be potentially exploited in terms of additional crush space. That potential benefit vanishes when higher BRC densities, like 100 g/l or more, are needed.

For straight impacts to the crown (constellations 1 and 8 - Fig. 7), where lower density BRCs are sufficient, the additional crush space can readily be exploited. For localized impacts (constellation 9), where higher density BRCs are needed to pass the test, the outer hardshell must be designed stiffer and/or stronger to limit local intrusions. In that way the outer hardshell would distribute the forces over a wider area of the foam, and subsequently the head, allowing to use lower density BRCs again.

4.2. Strain rate behaviour

The BRC foam shows a substantial strain rate amplification. Given that the structure can be considered an open-cell structure, this behaviour is surprisingly strong, and likely can be attributed to the viscoelasticity of the fibre itself [75,76], rather than to the load bearing of the entrapped gas and subsequent porous fluid flow. The strain rate effects become smaller, the higher the density of the BRC. This is also observed with EPS [77].

Over the first 30 % of strain, the average amplification reaches 2.9 and 4.3 at $300 \, s^{-1}$ and $700 \, s^{-1}$, respectively, for the 60 g/l BRC foam. In EPS foams of the same density the amplification averaged over the first 30 % of strain is considerably smaller, and amounts for roughly 1.5 [78] at $465 \, s^{-1}$. Generally, the strain-rate sensitivity increases with strain-rate, too. In foams (EPS, HDPE and PU) a transition strain-rate between 100 and $300 \, s^{-1}$ has been shown [78]. Therefore, additional elevated strain rate tests would be helpful to

identify the transition strain rate for the BRC.

The high strain rate tests indicate a non-constant amplification with strain: This has also been observed in other foams [77–79]. A high strain rate sensitivity is considered beneficial for head protection adaptive to a wide range of impact velocities [80,81]. However, the presumed source of strain rate dependency in BRC, viscoelasticity of the fibre, also suggests a high temperature sensitivity. Further, load rate effects are reduced, the higher the density of the foam. To fully exploit the load-rate effects of the structure, the foam should provide low density.

4.3. Foam density

The correlation between EPS foam density and peak linear accelerations was evident, while no such relationship was observed between density and angular velocity. The BRC helmet demonstrated exceptional performance in mitigating angular acceleration loads. The BRC foam exhibits lower strength at 10 % compression compared to EPS foams, suggesting its softer nature.

Initially, it was hypothesized that the rotational loading benefits of BRC foam were solely due to its reduced strength, implying that a lower-density EPS foam might offer comparable advantages. While angular accelerations did decrease with lower EPS foam densities, they did not achieve the low values observed with BRC foam.

This discrepancy can be attributed to the distinct mechanical properties of BRC foam, which lacks primary stiffness or strain softening [82]. In contrast, EPS foams exhibit high primary stiffness until cell wall buckling initiates, followed by strain softening. These fundamental differences in mechanical behaviour likely contribute to the superior performance of BRC foam in mitigating angular accelerations during impact scenarios.

On the other hand, high primary stiffness is beneficial in reducing crush depth (see supplementary material). This possibly indicates that a serial combination of foams would be beneficial to combine the requirements of reducing angular accelerations and reducing crushing depth. In terms of certification tests, it was surprising to find that lower density EPS foams were able to pass the EN 1078 certification test. It seems that the baseline helmet uses an unnecessarily dense foam.

4.4. Practical implications

Helmet manufacturers could incorporate BRC or similar materials in areas most susceptible to oblique impacts, potentially creating hybrid designs that combine the strengths of both BRC and traditional materials. The promising results of BRC could spur further research into sustainable, bio-based materials for helmet construction. However, this will require better control of material homogeneity in the production process, which in this study was still at laboratory scale. This study focused only on the impact attenuation performance of the helmet. UV stability, chemical resistance and the effects of temperature and humidity cycles have not been investigated. As BRC is a hydrophilic material, additional modification of the foam is required to limit the absorption of sweat and rain [83].

5. Conclusion

Bulky cellulosic network structures, BRC, with densities between 60 and 130 g/l, were used as an impact liner in a hardshell helmet. BRC was characterized over a wide range of strain rates in compression. A material card of the BRC foam was established – and validated against headform drop tests. The BRC material model was assigned to the impact liner of a validated hardshell helmet. The helmet was virtually tested in impact constellations representative of consumer information and certification tests. The measured kinematics and associated injury criteria were compared to a baseline helmet equipped with an impact liner made from EPS with a density of 70 g/l. Additionally, variations in helmet shape and EPS foam density were investigated.

It was found that the BRC outperforms the EPS helmet in oblique impacts, i.e. cases where the rotation is induced by tangential velocity – but is worse in straight impacts. Especially in oblique impacts inducing z-axis rotations, the BRC helmet is able to reduce angular accelerations and velocity changes by approx. 1/3. Similarly, the injury risk associated to angular motion is reduced by up to 90 %. In the tests inspired by consumer tests, the BRC (100 g/l) showed an average risk for sustaining AIS2 of 8 % and an average risk of concussion of 34 %. In the EPS helmet the respective values were 13 % and 46 %. However, the BRC helmet suffers from bottoming out in straight impacts with little overlap between impact liner and head, which is for example the case in impacts near the helmet's rim. This is aggravated by the low thickness of the helmet under study. As a result, the BRC helmet would not pass the certification when tested against the front of the helmet. This limitation was found to be easily overcome, for example by changing the helmet design and making the foam thicker at the front.

The results in the virtual consumer tests indicate that softer foams (like BRC) would be more beneficial than those used in conventional impact liners: These seem to prevent form-locking (between head and helmet) in z-rotation cases, that likely cannot be tackled with slip liners for simple geometric reasons ("form-locking").

In summary, it has been shown that cellulosic fibre network structures have the potential to replace fossil-based foams for impact energy management and injury prevention in bicycle helmets, and would provide an adequate level of protection.

6. Outlook

Further research should focus on improving the homogeneity of Bulky Cellulosic Network Structures (BRC), reducing their mechanical coefficient of variation, and addressing moisture absorption issues and investigating aging effects. These enhancements will

ensure that BRC not only effectively manages impact energy but also meets the comprehensive needs of end-users and industry standards.

7. Limitations

The cellulosic network structures BRC were shown to be orthotropic [69] – in terms of morphology and mechanics. It was further shown that the samples are inhomogeneous in terms of density in thickness directions. The orthotropies, but also density in-homogeneities arise from the manual manufacturing process, e.g., due to the pouring and spreading of the pulp into the mould – but also from skin formation in the drying process. In this study, though, it was assumed that the material is isotropic and homogenous.

CRediT authorship contribution statement

Florian Feist: Writing – original draft, Visualization, Validation, Supervision, Software, Project administration, Methodology, Investigation, Formal analysis, Data curation, Conceptualization. **Markus Wagner:** Writing – review & editing, Investigation, Formal analysis, Data curation. **Georg Baumann:** Writing – review & editing, Investigation, Formal analysis, Data curation. **Stefan Spirk:** Writing – review & editing, Methodology, Conceptualization. **Veronika Biegler:** Writing – review & editing, Resources. **Qixiang Jiang:** Writing – review & editing, Resources, Project administration. **Tiina Nypelö:** Writing – review & editing, Funding acquisition, Conceptualization.

Declaration of competing interest

The authors declare that they have no known competing financial interests or personal relationships that could have appeared to influence the work reported in this paper.

Appendix A. Supplementary data

Supplementary data related to this article can be found at https://doi.org/10.1016/j.heliyon.2024.e40790.

References

[1] H. Vahid Alizadeh, M.G. Fanton, A.G. Domel, G. Grant, D.B. Camarillo, A computational study of liquid shock absorption for prevention of traumatic brain injury, J. Biomech. Eng. 143 (2021), https://doi.org/10.1115/1.4049155.
[2] A. Bucker, H. Westerlaan, A. Mazuri, M. Uyttenboogaart, R. Smithuis, Traumatic Intracranial Hemorrhage, 2020.
[3] T.J. Orr, E. Lesha, A.H. Kramer, A. Cecia, J.E. Dugan, B. Schwartz, S.L. Einhaus, Traumatic brain injury: a comprehensive review of biomechanics and molecular pathophysiology, World Neurosurg 185 (2024) 74–88, https://doi.org/10.1016/j.wneu.2024.01.084.
[4] D.F. Meaney, B. Morrison, C. Dale Bass, The mechanics of traumatic brain injury: a review of what we know and what we need to know for reducing its societal burden, J. Biomech. Eng. 136 (2014) 21008, https://doi.org/10.1115/1.4026364.
[5] C.E. Keating, D.K. Cullen, Mechanosensation in traumatic brain injury, Neurobiol. Dis. 148 (2021) 105210, https://doi.org/10.1016/j.nbd.2020.105210.
[6] A. Holbourn, Mechanics of head injury, Lancet 242 (1943) 438–441, https://doi.org/10.1016/s0140-6736(00)87453-x.
[7] M. Razzaghi, Mechanical analysis of head impact, OAJNN 10 (2019), https://doi.org/10.19080/OAJNN.2019.10.555787.
[8] T.A. Gennarelli, L.E. Thibault, A.K. Ommaya, Pathophysiologic responses to rotational and translational accelerations of the head, in: SAE Technical Paper Series, SAE International400 Commonwealth Drive, Warrendale, PA, United States, 1972.
[9] N. Bourdet, C. Deck, T. Serre, C. Perrin, M. Llari, R. Willinger, In-depth real-world bicycle accident reconstructions, INT J CRASHWORTHINES 19 (2013) 222–232, https://doi.org/10.1080/13588265.2013.805293.
[10] P. Verschueren, Biomechanical Analysis of Head Injuries Related to Bicycle Accidents and a New Bicycle Helmet Concept (Biomechanische Analyse Van Hoofdletsels …, Leuven, Belgium, 2009.
[11] S. Kleiven, Why most traumatic brain injuries are not caused by linear acceleration but skull fractures are, Front. Bioeng. Biotechnol. 1 (2013) 15, https://doi.org/10.3389/fbioe.2013.00015.
[12] T. Skandsen, K.A. Kvistad, O. Solheim, I.H. Strand, M. Folvik, A. Vik, Prevalence and impact of diffuse axonal injury in patients with moderate and severe head injury: a cohort study of early magnetic resonance imaging findings and 1-year outcome, J. Neurosurg. 113 (2010) 556–563, https://doi.org/10.3171/2009.9.JNS09626.
[13] D.H. Smith, R. Hicks, J.T. Povlishock, Therapy development for diffuse axonal injury, J. Neurotrauma 30 (2013) 307–323, https://doi.org/10.1089/neu.2012.2825.

[14] J.E. Greer, J.T. Povlishock, K.M. Jacobs, Electrophysiological abnormalities in both axotomized and nonaxotomized pyramidal neurons following mild traumatic brain injury, J. Neurosci. 32 (2012) 6682–6687, https://doi.org/10.1523/JNEUROSCI.0881-12.2012.

[15] E.D. Bigler, W.L. Maxwell, Neuropathology of mild traumatic brain injury: relationship to neuroimaging findings, Brain Imaging Behav 6 (2012) 108–136, https://doi.org/10.1007/s11682-011-9145-0.

[16] J.C. Park, I.B. Chang, J.H. Ahn, J.H. Kim, J.K. Oh, J.H. Song, Epidemiology and risk factors for bicycle-related severe head injury: a single center experience, Korean J. Neurotrauma 13 (2017) 90–95, https://doi.org/10.13004/kjnt.2017.13.2.90.

[17] J. Olivier, I. Radun, Bicycle helmet effectiveness is not overstated, Traffic Inj. Prev. 18 (2017) 755–760, https://doi.org/10.1080/15389588.2017.1298748.

[18] A. Hoye, Recommend or mandate? A systematic review and meta-analysis of the effects of mandatory bicycle helmet legislation, Accid. Anal. Prev. 120 (2018) 239–249, https://doi.org/10.1016/j.aap.2018.08.001.

[19] M. Bíl, M. Dobiáš, R. Andrášik, M. Bílová, P. Hejna, Cycling fatalities: when a helmet is useless and when it might save your life, Saf. Sci. 105 (2018) 71–76, https://doi.org/10.1016/j.ssci.2018.02.005.

[20] M. Fahlstedt, P. Halldin, S. Kleiven, The protective effect of a helmet in three bicycle accidents–A finite element study, Accid. Anal. Prev. 91 (2016) 135–143, https://doi.org/10.1016/j.aap.2016.02.025.

[21] Y. Matsui, S. Oikawa, N. Hosokawa, Effectiveness of wearing a bicycle helmet for impacts against the front of a vehicle and the road surface, Traffic Inj. Prev. 19 (2018) 773–777, https://doi.org/10.1080/15389588.2018.1498089.

[22] A. Vyas, A. Grigorian, C.M. Kuza, M. Dolich, V. Joe, T. Chin, J. Nahmias, Adult bicycle collisions: impact of helmet use on head and cervical spine injury, J. Surg. Res. 258 (2021) 307–313, https://doi.org/10.1016/j.jss.2020.08.042.

[23] E.J. Alfrey, M. Tracy, J.R. Alfrey, M. Carroll, E.D. Aranda-Wikman, T. Arora, J. Maa, J. Minnis, Helmet usage reduces serious head injury without decreasing concussion after bicycle riders crash, J. Surg. Res. 257 (2021) 593–596, https://doi.org/10.1016/j.jss.2020.08.009.

[24] C. Klug, F. Feist, E. Tomasch, CLEVERER HELM - Optimaler Schutz vor Kopfverletzungen durch verbesserte Testmethoden von Kinder-Fahrradhelmen, Wien, 2015.

[25] F. Feist, C. Klug, A numerical study on the influence of the upper body and neck on head kinematics in tangential bicycle helmet impact, in: 2016 IRCOBI Conference Proceedings, Malaga, Spain, IRCOBI, 2016, pp. 162–184. https://www.ircobi.org/wordpress/downloads/irc16/pdf-files/28.pdf.

[26] C. Deck, N. Bourdet, F. Meyer, R. Willinger, Protection performance of bicycle helmets, J. Saf. Res. 71 (2019) 67–77, https://doi.org/10.1016/j.jsr.2019.09.003.

[27] M.L. Bland, C. McNally, D.S. Zuby, B.C. Mueller, S. Rowson, Development of the STAR evaluation system for assessing bicycle helmet protective performance, Ann. Biomed. Eng. 48 (2020) 47–57, https://doi.org/10.1007/s10439-019-02330-0.

[28] H. Stigson, M. Rizzi, A. Ydenius, E. Engström, A. Kullgren, Consumer Testing of Bicycle Helmets, Conference Proceeding of the International Research Council of the Biomechanics of Impact (IRCOBI) Conference, 2017, pp. 1–9.

[29] M. Fahlstedt, Sammanställning Av Utvärdering Av Olika Huvudskydd För Cyklister 2021, 2021.

[30] N. Lindgren, P. Halldin, M. Fahlstedt, Influence of headform on assessments and ratings of the protective performance of bicycle helmets. IRC-22-107, in: 2022 IRCOBI Conference Proceedings, 2022, pp. 1–20. Porto, Portugal, IRCOBI.

[31] J. Versace, A review of the severity Index, in: 15th Stapp Car Crash Conference Proceedings, SAE International, Coronado, CA, 1971.

[32] M. Fahlstedt, F. Abayazid, M.B. Panzer, A. Trotta, W. Zhao, M. Ghajari, M.D. Gilchrist, S. Ji, S. Kleiven, X. Li, A.N. Annaidh, P. Halldin, Ranking and rating bicycle helmet safety performance in oblique impacts using eight different brain injury models, Ann. Biomed. Eng. 49 (2021) 1097–1109, https://doi.org/10.1007/s10439-020-02703-w.

[33] R. Eppinger, E. Sun, F. Bandak, M. Haffner, N. Khaewpong, M. Maltese, S. Kuppa, T. Nguyen, E. Takhounts, R. Tannous, A. Zhang, R. Saul, Development of Improved Injury Criteria for the Assessment of Advanced Automotive Restraint Systems - II, 1999.

[34] J.A. Newman, A generalized acceleration model for brain injury threshold (GAMBIT), in: 1986 IRCOBI Conference Proceedings, 1986, pp. 121–131. Zurich (Switzerland), IRCOBI.

[35] S. Kleiven, Influence of impact direction on the human head in prediction of subdural hematoma, J. Neurotrauma 20 (2003) 365–379, https://doi.org/10.1089/089771503765172327.

[36] E.G. Takhounts, M.J. Craig, K. Moorhouse, J. McFadden, V. Hasija, Development of brain injury criteria (BrIC), Stapp Car Crash J 57 (2013) 243–266.

[37] L.F. Gabler, J.R. Crandall, M.B. Panzer, Development of a metric for predicting brain strain responses using head kinematics, Ann. Biomed. Eng. 46 (2018) 972–985, https://doi.org/10.1007/s10439-018-2015-9.

[38] C.W. Gadd, Use of a weighted-impulse criterion for estimating injury hazard, in: 10th Stapp Car Crash Conference Proceedings, Hollomon Air Force Base, NM, SAE International, 1966.

[39] J. Newman, C. Barr, M.C. Beusenberg, E. Fournier, N. Shewchenko, E. Welbourne, C. Withnall, A new biomechanical assessment of mild traumatic brain injury. Part 2: results and conclusions, in: 2000 IRCOBI Conference Proceedings, Montpellier (France), IRCOBI, 2000.

[40] M. Vander Vorst, J. Stuhmiller, K. Ho, N. Yoganandan, F. Pintar, Statistically and biomechanically based criterion for impact-induced skull fracture, Annu. Proc. Assoc. Adv. Automot. Med. 47 (2003) 363–381.

[41] S. Kleiven, Predictors for traumatic brain injuries evaluated through accident reconstructions, Stapp Car Crash J 51 (2007) 81–114.

[42] R.M. Greenwald, J.T. Gwin, J.J. Chu, J.J. Crisco, Head impact severity measures for evaluating mild traumatic brain injury risk exposure, Neurosurgery 62 (2008) 789, https://doi.org/10.1227/01.neu.0000318162.67472.ad.

[43] E.G. Takhounts, V. Hasija, S.A. Ridella, S. Rowson, S.M. Duma, Kinematic rotational brain injury criterion (BRIC), in: The 22nd ESV Conference Proceedings, Washington, D.C., USA, NHTSA, 2011.

[44] H. Kimpara, M. Iwamoto, Mild traumatic brain injury predictors based on angular accelerations during impacts, Ann. Biomed. Eng. 40 (2012) 114–126, https://doi.org/10.1007/s10439-011-0414-2.

[45] S. Rowson, S.M. Duma, Brain injury prediction: assessing the combined probability of concussion using linear and rotational head acceleration, Ann. Biomed. Eng. 41 (2013) 873–882, https://doi.org/10.1007/s10439-012-0731-0.

[46] T. Yanaoka, Y. Dokko, Y. Takahashi, Investigation on an injury criterion related to traumatic brain injury primarily induced by head rotation, SAE technical papers series. https://doi.org/10.4271/2015-01-1439, 2015.

[47] Y. Takahashi, T. Yanaoka, A study of injury criteria for brain injuries in traffic accidents. 25th International Technical Conference on the Enhanced Safety of Vehicles (ESV), National Highway Traffic Safety, Administration, 2017, in: https://www-esv.nhtsa.dot.gov/Proceedings/25/25ESV-000040.pdf.

[48] L.F. Gabler, J.R. Crandall, M.B. Panzer, Assessment of kinematic brain injury metrics for predicting strain responses in diverse automotive impact conditions, Ann. Biomed. Eng. (2016) 1–14, https://doi.org/10.1007/s10439-016-1697-0.

[49] M.L. Bland, C. McNally, S. Rowson, Differences in impact performance of bicycle helmets during oblique impacts, J. Biomech. Eng. 140 (2018), https://doi.org/10.1115/1.4040019.

[50] R.M. Coelho, R.J. Alves de Sousa, F. Fernandes, F. Teixeira-Dias, New composite liners for energy absorption purposes, Mater. Des. 43 (2013) 384–392, https://doi.org/10.1016/j.matdes.2012.07.020.

[51] R.A. de Sousa, R. Gonçalves, R. Coelho, F. Teixeira-Dias, Assessing the effectiveness of a natural cellular material used as safety padding material in motorcycle helmets, Simulation 88 (2012) 580–591, https://doi.org/10.1177/0037549711414735.

[52] R. Clouard, How Eco-Design Tools Can Be Implemented in the Product Development Process of a Company: A Case Study on Bicycle Helmet, Master Thesis, Aalto, 2021.

[53] L. Chang, Y. Guo, X. Huang, Y. Xia, Z. Cai, Experimental study on the protective performance of bulletproof plate and padding materials under ballistic impact, Mater. Des. 207 (2021) 109841, https://doi.org/10.1016/j.matdes.2021.109841.

[54] Y. Xu, Le Tang, C. Nok-Iangthong, M. Wagner, G. Baumann, F. Feist, A. Bismarck, Q. Jiang, Functionally gradient macroporous polymers: emulsion templating offers control over density, pore morphology, and composition, ACS Appl. Polym. Mater. 6 (2024) 5150–5162, https://doi.org/10.1021/acsapm.4c00261.

[55] X. Huang, Q. Zheng, L. Chang, Z. Cai, Study on protective performance and gradient optimization of helmet foam liner under bullet impact, Sci. Rep. 12 (2022) 16061, https://doi.org/10.1038/s41598-022-20533-9.

[56] J. Abderezaei, F. Rezayaraghi, B. Kain, A. Menichetti, M. Kurt, An overview of the effectiveness of bicycle helmet designs in impact testing, Front. Bioeng. Biotechnol. 9 (2021) 718407, https://doi.org/10.3389/fbioe.2021.718407.

[57] A. Surabhi, Abus Kranium. http://anirao.com/project_helmets/project_helmets_page1.php.

[58] S.R. McQuade. Recyclable Disposable Helmet Design, 2015. https://sear.unisq.edu.au/29290/1/McQuade_S_Malpress.pdf.

[59] B. Petersen, Paper pulp helmet. https://www.bobbypetersen.com/paper-pulp-helmet, 2013.

[60] I. Shiffer, EcoHelmet: a folding, recycable helmet for bike share. https://www.ecohelmet.com/, 2017.

[61] K. Hwang, H. Kim, M. Al-Rawi, S. Kim, Designing foldable helmets for micro-mobility using sustainable materials, adr 36 (2023) 129–143, https://doi.org/10.15187/adr.2023.05.36.2.129.

[62] A. Ek, Bicycle helmet form the forest. https://wwsc.se/bicycle-helmet-from-the-forest/, 2015.

[63] F. Fernandes, R. Alves de Sousa, M. Ptak, G. Migueis, Helmet design based on the optimization of biocomposite energy-absorbing liners under multi-impact loading, Appl. Sci. 9 (2019) 735, https://doi.org/10.3390/app9040735.

[64] F. Fernandes, R.T. Jardin, A.B. Pereira, R.J. Alves de Sousa, Comparing the mechanical performance of synthetic and natural cellular materials, Mater. Des. 82 (2015) 335–341, https://doi.org/10.1016/j.matdes.2015.06.004.

[65] S. Gürgen, F.A.O. Fernandes, R.J.A. de Sousa, M.C. Kuşhan, Development of eco-friendly shock-absorbing cork composites enhanced by a non-Newtonian fluid, Appl. Compos. Mater. 28 (2021) 165–179, https://doi.org/10.1007/s10443-020-09859-7.

[66] P. Kaczynski, M. Ptak, J. Wilhelm, F. Fernandes, R.A. de Sousa, High-energy impact testing of agglomerated cork at extremely low and high temperatures, Int. J. Impact Eng. 126 (2019) 109–116, https://doi.org/10.1016/j.ijimpeng.2018.12.001.

[67] M. Ptak, P. Kaczynski, F. Fernandes, R.A. de Sousa, Assessing impact velocity and temperature effects on crashworthiness properties of cork material, Int. J. Impact Eng. 106 (2017) 238–248, https://doi.org/10.1016/j.ijimpeng.2017.04.014.

[68] M. Gerometta, X. Gabrion, A. Lagorce, S. Thibaud, T. Karbowiak, Towards better understanding of the strain–stress curve of cork: a structure–mechanical properties approach, Mater. Des. 235 (2023) 112376, https://doi.org/10.1016/j.matdes.2023.112376.

[69] M. Wagner, V. Biegler, S. Wurm, G. Baumann, A. Bismarck, F. Feist. Pulp fibre foams: Morphology and mechanical performance, 2024, https://doi.org/10.1016/j.compositesa.2024.108515. Graz, Wien, Austria.

[70] F.S. Chang, Y. Song, D.X. Lu, C.N. DeSilva, Unified constitutive equations of foam materials, J. Eng. Mater. Technol. 120 (1998) 212–217, https://doi.org/10.1115/1.2812345.

[71] Livermore Software Technology Corporation, LS-DYNA Keyword User's Manual: Volume II, Material Models. LS-DYNA R7.1, Livermore, California, 2014.

[72] F. Feist, C. Klug. Bicycle Helmet (LS-Dyna), 2022. https://openvt.eu/fem/bicycle-helmet.

[73] Ellway J., Sandner V., Eggers A., Masuda M., Brain Injury Calculation: Technical Bulletin TB,, (2022) 035. Version 1.0,. https://cdn.euroncap.com/media/67886/tb-035-brain-injury-calculation-v10.pdf.

[74] M.F. Ashby, The properties of foams and lattices, Philos. Trans. A Math. Phys. Eng. Sci. 364 (2006) 15–30, https://doi.org/10.1098/rsta.2005.1678.

[75] G. Baumann, C. Czibula, U. Hirn, F. Feist, A digital-twin driven Split Hopkinson bar layout for the tensile characterization of thin, low impedance, sheet-like materials, Int. J. Impact Eng. 194 (11) (2024) 105098, https://doi.org/10.1016/j.ijimpeng.2024.105098.

[76] G. Baumann, C. Czibula, U. Hirn, F. Feist, The tensile behaviour of paper under high loading rates, Cellulose (2025) 6266, https://doi.org/10.1007/s10570-024-06266-0.

[77] W.-J. Kang, S.-S. Cheon, I.-H. Lee, S.-U. Choi, J.-H. Min, S.-H. Lee, B.-K. Bae, Investigation of the strain rate effects of EPS foam, Journal of The Korean Society for Composite Materials 23 (2010) 64–68, https://doi.org/10.7234/kscm.2010.23.3.064.

[78] S. Ouellet, D. Cronin, M. Worswick, Compressive response of polymeric foams under quasi-static, medium and high strain rate conditions, Polym. Test. 25 (2006) 731–743, https://doi.org/10.1016/j.polymertesting.2006.05.005.

[79] D.S. Cronin, S. Ouellet, Low density polyethylene, expanded polystyrene and expanded polypropylene: strain rate and size effects on mechanical properties, Polym. Test. 53 (2016) 40–50, https://doi.org/10.1016/j.polymertesting.2016.04.018.

[80] J. Kunecky, O. Jirousek. Study of possible use of strain-rate dependent materials in protective helmets, Inc, Providence, Rhode Island, USA, 2010.

[81] C. Bradfield, N. Vavalle, B. DeVincentis, E. Wong, Q. Luong, L. Voo, C. Carneal, Combat helmet suspension system stiffness influences linear head acceleration and white matter tissue strains: implications for future helmet design, Mil. Med. 183 (2018) 276–286, https://doi.org/10.1093/milmed/usx181.

[82] M. Wagner, V. Biegler, S. Wurm, G. Baumann, T. Nypelö, A. Bismarck, F. Feist, Pulp fibre foams: morphology and mechanical performance, Compos. Appl. Sci. Manuf. (2025) 108515, https://doi.org/10.1016/j.compositesa.2024.108515.

[83] F. Feist. Foam Applicability in the Automotive Sector: Deliverable 5.1, Brussels, 2024. https://www.breadcell.eu/images/media/D51.pdf.

[84] T. Pöhler, J.A. Ketoja, T. Lappalainen, V.-M. Luukkainen, I. Nurminen, P. Lahtinen, K. Torvinen, On the strength improvement of lightweight fibre networks by polymers, fibrils and fines, Cellulose 27 (2020) 6961–6976. https://doi.org/10.1007/s10570-020-03263-x.

[85] E. Orzan. Upgrading Cellulose Networks: Conquering Limitations in Fiber Foams, Göteborg, 2023. https://research.chalmers.se/publication/535930/file/535930_Fulltext.pdf.

[86] M. Wagner, S. Wurm, G. Baumann, F. Feist, T. Nypelö, Lost in Homogenisation: Navigating the Challenges of Predicting Ideal Behaviour in Inhomogeneous Porous Structures. Manuscript submitted for publication.

[87] N. Debabèche, M. Wagner, F. Feist, G. Baumann, Q. Jiang, A. Bismarck. All-cellulose stiffened Sandwich Composites, 2025. Manuscript in preparation.

[88] L. Cui, S. Kiernan, M.D. Gilchrist, Designing the energy absorption capacity of functionally graded foam materials, Mater. Sci. Eng. A 507 (2009) 215–225. https://doi.org/10.1016/j.msea.2008.12.011.

[89] M.W. Schraad, F.H. Harlow, A stochastic constitutive model for disordered cellular materials: Finite-strain uni-axial compression, Int. J. Solids. Struct. 43 (2006) 3542–3568. https://doi.org/10.1016/j.ijsolstr.2005.05.018.

[90] Deutsches Institut für Normung e.V., Helme für Radfahrer und für Benutzer von Skateboards und Rollschuhen; Deutsche Fassung EN 1078:2012+A1:2012, 2014 04. https://www.austrian-standards.at/de/shop/din-en-1078-2014-04~p2065083.

[91] H. Liu, H. Du, T. Zheng, K. Liu, X. Ji, T. Xu, X. Zhang, C. Si, Cellulose based composite foams and aerogels for advanced energy storage devices, Chem. Eng. J. 426 (2021) 130817. https://doi.org/10.1016/j.cej.2021.130817.

[92] T. Budtova, Bio-based aerogels: a new generation of thermal superinsulating materials, in: T. Rosenau, A. Potthast, J. Hell (Eds.), Cellulose science and technology: chemistry, analysis, and applications, First edition, John Wiley & Sons, Hoboken, NJ, 2019, pp. 371–392.

[93] D. Klemm. Fundamentals and analytical methods, Wiley-VCH, Weinheim, 1998.

[94] J.-O. Yeon, K.-W. Kim, K.-S. Yang, J.-M. Kim, M.-J. Kim, Physical properties of cellulose sound absorbers produced using recycled paper, Construct. Build. Mater. 70 (2014) 494, 50.

[95] T. Hjelt, J.A. Ketoja, H. Kiiskinen, A.I. Koponen, E. Pääkkönen, Foam forming of fiber products: a review, J. Dispers. Sci. Technol. 55 (2021) 1–37. https://doi.org/10.1080/01932691.2020.1869035.

[96] P. Nechita, S.M. Năstac, Overview on foam forming cellulose materials for cushioning packaging applications, Polymers 14 (2022). https://doi.org/10.3390/polym14101963.

[97] G. Baumann, D. Niederkofler, C. Ellersdorfer, F. Feist, On the development of a release mechanism for a split Hopkinson tension and compression bar, Materials 14 (2021). https://doi.org/10.3390/ma14247609.